



ARTICLE

<https://doi.org/10.1038/s41467-019-13023-6>

OPEN

Atomic mechanism of strong interactions at the graphene/sapphire interface

Zhipeng Dou^{1,2,11}, Zhaolong Chen^{3,11}, Ning Li^{1,4,11}, Shenyuan Yang^{5,6*}, Zhiwei Yu⁷, Yuanwei Sun^{1,4}, Yuehui Li^{1,4}, Bingyao Liu¹, Qiang Luo⁴, Tianbao Ma⁷, Lei Liao^{2*}, Zhongfan Liu^{3,8}  & Peng Gao^{1,4,9,10*} 

For atomically thin two-dimensional materials, interfacial effects may dominate the entire response of devices, because most of the atoms are in the interface/surface. Graphene/sapphire has great application in electronic devices and semiconductor thin-film growth, but the nature of this interface is largely unknown. Here we find that the sapphire surface has a strong interaction with some of the carbon atoms in graphene to form a C-O-Al configuration, indicating that the interface interaction is no longer a simple van der Waals interaction. In addition, the structural relaxation of sapphire near the interface is significantly suppressed and very different from that of a bare sapphire surface. Such an interfacial C-O-Al bond is formed during graphene growth at high temperature. Our study provides valuable insights into understanding the electronic structures of graphene on sapphire and remote control of epitaxy growth of thin films by using a graphene-sapphire substrate.

¹Electron Microscopy Laboratory, School of Physics, Peking University, Beijing 100871, China. ²Key Laboratory for Micro-/Nano-Optoelectronic Devices of Ministry of Education, School of Physics and Electronics, Hunan University, Changsha 410082, China. ³Center for Nanochemistry (CNC), Beijing Science and Engineering Center for Nanocarbons, College of Chemistry and Molecular Engineering, Peking University, Beijing 100871, China. ⁴International Center for Quantum Materials, Peking University, Beijing 100871, China. ⁵State Key Laboratory of Superlattices and Microstructures, Institute of Semiconductors, Chinese Academy of Sciences, Beijing 100083, China. ⁶Center of Materials Science and Optoelectronics Engineering, University of Chinese Academy of Science, Beijing 100049, China. ⁷State Key Laboratory of Tribology, Tsinghua University, Beijing 100084, China. ⁸Beijing Graphene Institute (BGI), Beijing 100095, China. ⁹Collaborative Innovation Center of Quantum Matter, Beijing 100871, China. ¹⁰Beijing Key Laboratory of Quantum Devices, Beijing 100871, China. ¹¹These authors contributed equally: Zhipeng Dou, Zhaolong Chen, and Ning Li. *email: syyang@semi.ac.cn; liaolei@whu.edu.cn; p-gao@pku.edu.cn

The interface is the device¹. At the interface of crystal materials, the broken translation symmetry usually strongly alters the optical, electric, and magnetic properties, resulting in many interesting phenomena such as interface-induced superconductivity^{2,3}, two-dimensional (2D) electron gas⁴, and magnetoelectric coupling^{5,6}. In particular, the interface effects are much more pronounced or dominant in atomically thin 2D materials (e.g., graphene (Gr)), because most of the atoms are part of the interface when supported on a substrate. For instance, in a field-effect transistor system, strong hybridization (orbital overlap) between 2D materials and contact metals can eliminate the van der Waals (vdW) gap, which results in a reduction of the tunnel barrier for carriers⁷. Such an effect is also observed in 2D/2D heterostructures, e.g., the topological current is detected in the Gr/h-BN superlattice⁸ and the reconstruction at the Gr/h-BN interface provides a periodic scattering potential for carriers, leading to very unique electrical properties⁹. Moreover, coupling of the Gr/Gr interface via the “magic” angle results in correlated insulating states at half-filling¹⁰ and can be tuned to zero-resistance states upon electrostatic doping¹¹.

Recently, Gr/sapphire (α -Al₂O₃) has shown promising applications in electronic devices due to the relatively high dielectric properties of α -Al₂O₃ as a gate dielectric^{12,13}. In addition, Gr/ α -Al₂O₃ is also applied as a platform for remote growth of third-generation semiconductors where Gr acts as a buffer layer to overcome the limitation of lattice mismatch^{14–16}. The penetration of the electrostatic potential from substrates is governed by the interface nature, which eventually determines the epitaxial crystal quality^{17,18}. Therefore, it is vital to reveal the atomic structure and binding nature of the Gr/ α -Al₂O₃ interface^{19,20}. Although considerable advances have been achieved in characterization techniques, little is known about the structure and properties of the Gr/ α -Al₂O₃ system because of the lack of effective methods to probe the atomically thin interface of Gr on insulating substrates. For instance, the common scanning tunneling microscopy and low-energy electron diffraction (LEED) methods are usually restricted to conductive substrates, but α -Al₂O₃ is nonconductive. Therefore, most of the previous knowledge is obtained from computational approaches such as density functional theory (DFT) calculations²¹. Aberration-corrected transmission electron microscopy (Cs-TEM), which enables atomically resolved identification of the structure and chemical composition of materials regardless of their electric conductivity, provides alternative opportunities to study the atomic structure and properties of the interface and surface for insulators^{22,23}.

Here, by Cs-TEM, we successfully reveal the atomic arrangement of the Gr/ α -Al₂O₃ interface and accurately measure the gap between Gr and α -Al₂O₃, which governs the interaction between the substrate and functional layers. We observe that the atomic configuration at the interface is C-O-Al, which is further confirmed by DFT calculations. Such an interfacial bond induces a large adhesion energy of ~ 1.47 J/m², indicating that the interaction of the Gr/ α -Al₂O₃ interface is no longer a simple vdW interaction. In addition, we also precisely obtain the structural relaxation of the surface layers of α -Al₂O₃ and find that the structure of Al₂O₃ near the interface is significantly different than either the bulk or bare α -Al₂O₃ surface. The contraction rate of the first Al layer at the interface is $-(35.3 \pm 8.2)\%$ with respect to the bulk value compared with -79.4% for a bare α -Al₂O₃ surface. The pristine surface of α -Al₂O₃ is further identified to be Al-terminated and the interfacial C-O-Al bond is likely formed during high-temperature growth of Gr. All these findings provide valuable insights into the binding nature between 2D materials on a substrate and would be beneficial to the strategy of remote epitaxial growth by using a Gr buffer layer.

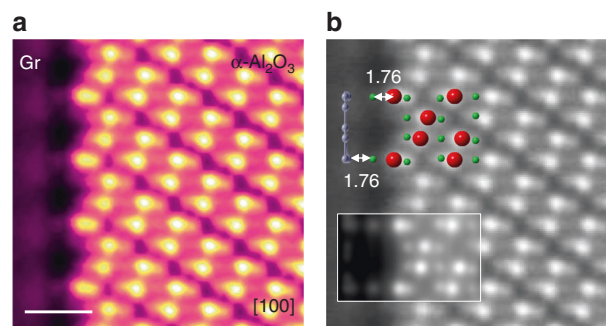


Fig. 1 Atomic structure of the Gr/ α -Al₂O₃ interface. **a** HAADF image viewing along the [100] orientation. The image is colored to clearly show the interface structure. **b** The corresponding ball and stick model and simulated image. The unit of length is Å. Scale bar: 0.5 nm. Red: Al atom. Green: O atom. Gray: C atom

Results

Characterization of the Gr/ α -Al₂O₃ interface. To ensure the cleanness of the interface, we directly grew a Gr film on α -Al₂O₃ substrates via a chemical vapor deposition (CVD) method (see details in the Methods section). For better protection of the Gr/ α -Al₂O₃ interface, a multilayer Gr film was obtained by prolonging the growth time. Raman mappings of I_G and I_{2D} of the obtained Gr/ α -Al₂O₃ in Supplementary Fig. 1a, b show a high uniform color contrast at the microscale, indicating the uniformity of the grown Gr film. The relatively low value of I_{2D}/I_G (≤ 0.8) confirms the multilayer feature of Gr (Supplementary Fig. 1c). Moreover, the G and 2D peaks of CVD-derived Gr/ α -Al₂O₃ are all upshifted with respect to those of transferred Gr on SiO₂/Si substrates (Supplementary Fig. 1d), indicating that Gr experiences a compressive strain imposed by α -Al₂O₃.

We used the high-angle annular dark-field scanning TEM (HAADF-STEM) imaging mode of Cs-TEM to reveal the atomic structure of the Gr/ α -Al₂O₃ interface. The atomically resolved image of the Gr/ α -Al₂O₃ interface with a viewing direction of [100] is shown in Fig. 1a and the Gr layer can be clearly observed in an image with lower magnification in Supplementary Fig. 2. The corresponding atomic structures of α -Al₂O₃ and Gr are depicted in Fig. 1b from the [100] direction superimposed on the STEM image and are in good agreement with the simulated result. We observe additional atoms between the Gr layer and the topmost surface Al atoms. These atoms are further identified to be O, which will be explained later in detail. The distance between the topmost surface Al and the additional O is ~ 1.76 Å, whereas the spacing between the O and the Gr is also ~ 1.76 Å, indicating a strong interaction between Gr and the α -Al₂O₃ substrate.

The presence of the C–O bond at the interface is further confirmed by the C 1s X-ray photoelectron spectroscopy spectrum (Supplementary Fig. 3) of Gr/ α -Al₂O₃, which shows an intense sp^2 carbon peak (~ 284.8 eV), a weak C–H peak (~ 285.7 eV), and a weak C–O peak (~ 287.3 eV). Such a C–O peak suggests the existence of a C–O–Al configuration at the interface²⁴.

DFT calculation of the Gr/ α -Al₂O₃ interface. We perform DFT calculations to verify the Gr/ α -Al₂O₃ interface structures²¹. To construct the Gr/ α -Al₂O₃ interface, we first added an additional atom on top of the surface Al atom according to the STEM results and then added the Gr layer (Supplementary Methods for details). We consider all the possibilities (O, H, C, and Al) for the additional atoms and find that only the O atoms can produce an interface structure consistent with the experimental results, as shown in Supplementary Figs. 4–6. The structure without

additional atoms at the interface is also shown in Supplementary Fig. 7 for comparison. Figure 2a,b shows the top and side views, respectively, of the geometry of the Gr/ α -Al₂O₃ interface with the additional O atoms obtained from DFT calculations. The additional O atoms directly bond to some of the C atoms of Gr with a bond length of 1.400 Å, as shown in Fig. 2b, whereas the other C atoms are further away from the α -Al₂O₃ surface. As a result, the average spacing between the additional O atoms and the Gr is 1.762 Å, which is in good agreement with the experimental results.

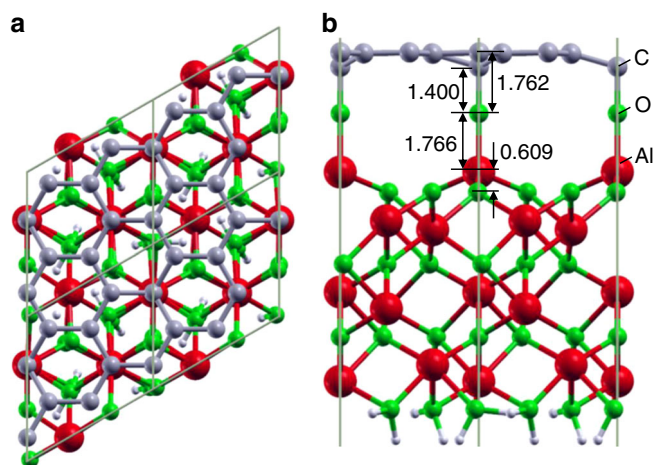


Fig. 2 Calculated interface structure of Gr/ α -Al₂O₃. **a** Top view. **b** Side view. The unit of length is Å. Red: Al atom. Green: O atom. Gray: C atom

Effects on the surface structure of α -Al₂O₃. Figure 3 shows the quantitative analysis of the surface structure of α -Al₂O₃ along the [100] orientation based on the image shown in Fig. 1a. We measured the distance between Al atoms from different layers (Al–Al length) and the angle between the Al–Al direction and the normal direction of the interface (Al–Al angle). There are negligible deviations of the Al–Al distance and angle far below the surface compared with bulk α -Al₂O₃, whereas a significant difference is observed for the top surface layers, as shown in Fig. 3a,c. In our experiment, the Al–Al distance at the surface is \sim 2.3 Å, which is in sharp contrast to the bulk value of \sim 2.6 Å. Furthermore, a similar trend is observed for the Al–Al angles, i.e., the angle at the surface is \sim 36°, whereas it is \sim 32.5° in the bulk. The DFT calculations also show a large change in surface relaxation for α -Al₂O₃, i.e., 2.22 Å for the Al–Al distance at the surface and 2.58 Å inside the bulk and 38.64° for the Al–Al angle at the surface and 32.39° inside the bulk, which is in excellent agreement with the experimental results.

Indeed, the structure relaxation at the surface is an important physical phenomenon in many materials^{25–27}, including α -Al₂O₃. We now compare the structure relaxation of α -Al₂O₃ near the interface with the bare surface case reported in the literatures in Fig. 4. In our case, the surface contraction is approximately $-(35.3 \pm 8.2)\%$ for the top layer (distance from the first Al layer to the second O layer) compared with the bulk, whereas the relaxation rates become $-(1.6 \pm 0.3)\%$, $-(27.1 \pm 10.5)\%$, $(16.6 \pm 2.9)\%$, and $-(8.2 \pm 1.6)\%$ for the second, third, fourth, and fifth layers, respectively. These measured values are very close to our DFT calculations and typically smaller than that of a bare α -Al₂O₃ surface reported in previous DFT calculations and experiments²¹, indicating that the strong interaction between the α -Al₂O₃ surface and the C atoms in Gr effectively suppresses the structure relaxation of the α -Al₂O₃ surface.

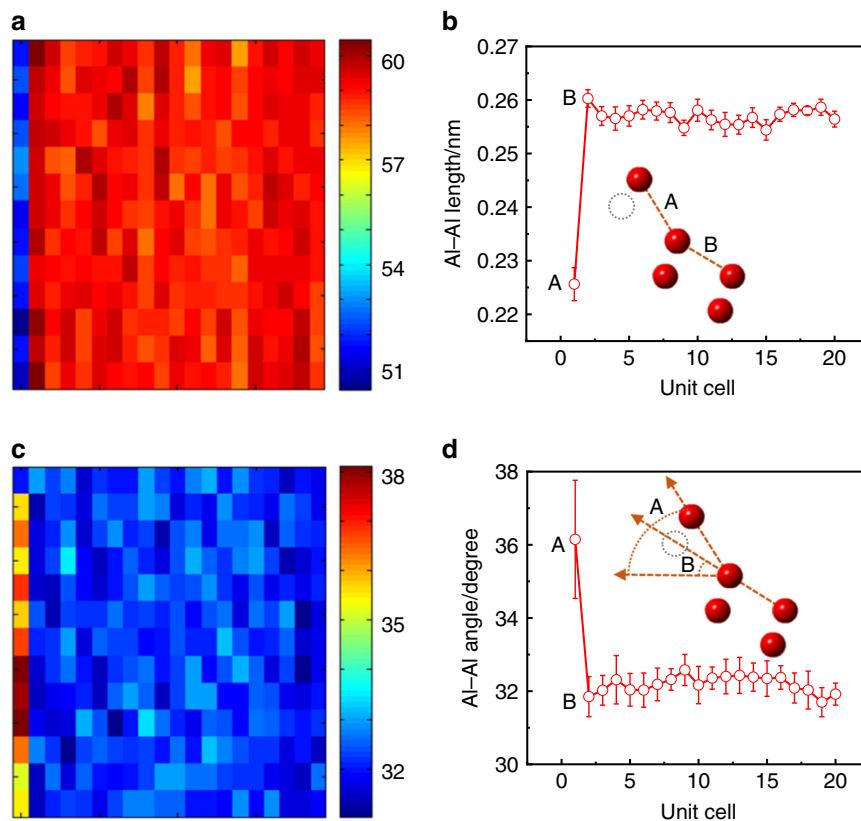


Fig. 3 Quantitative measurements of Al–Al length and angle. **a** Al–Al length mapping. **b** Averaged distance. **c** Al–Al angle mapping. **d** Averaged angle. The error bars are the standard deviation (SD)

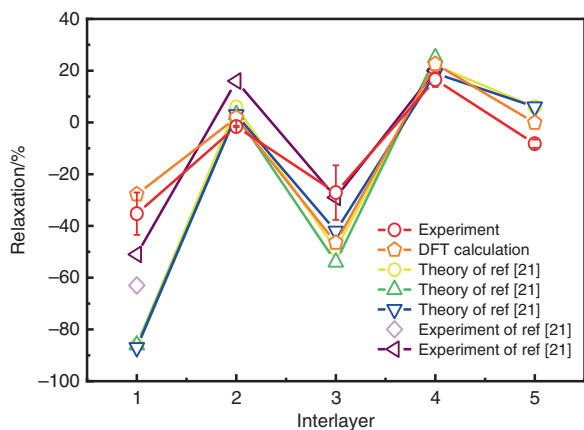


Fig. 4 Interlayer relaxation of α -Al₂O₃ in percent of the corresponding bulk spacings. The relaxation from the first layer (Al) to the second layer (O) is $-35.3 \pm 8.2\%$. The DFT calculation and previous results are also plotted for comparison. The error bar of experimental relaxation is calculated from the SD of bond length

Discussion

Thus far, we have obtained the atomic structure of the Gr/ α -Al₂O₃ interface and identified the C–O–Al bonding at the interface. It is a prerequisite to determine the pristine structure of the α -Al₂O₃ surface before growth of Gr to understand the formation of the C–O–Al interfacial structure. In fact, much effort has been made to reveal the surface structure of α -Al₂O₃, because it is widely used as a substrate for the growth of thin metals, high-temperature superconductors, 2D materials, and semiconductor films^{28–30}. Nevertheless, there are controversies regarding the termination layer of α -Al₂O₃. Both empirical and theoretical simulations identified only one stable Al-termination stoichiometry for the α -Al₂O₃ surface, whereas a few studies reported a stable O-termination structure²¹. A recent study of LEED measurements reported that the ratio of Al- to O-terminated domains is 2:1³¹.

We attempt to directly reveal the surface structure of pristine α -Al₂O₃ using the same Cs-TEM method, however, during the TEM specimen thinning process, the surface amorphization became severe, preventing us from identifying the termination layer of the pristine α -Al₂O₃ surface. We then transferred Gr onto α -Al₂O₃ to avoid any high-temperature process before the sample thinning process to protect the α -Al₂O₃ surface. We find that no bridging O atom is observed at the interface of the transferred Gr/ α -Al₂O₃, and that the surface of α -Al₂O₃ is Al-terminated in the ambient environment, as shown in Supplementary Fig. 8a. We also perform DFT calculations, which further confirm that the Al-termination layer is the most stable for the α -Al₂O₃ surface in Supplementary Fig. 9.

Therefore, it seems that during high-temperature growth of Gr, the O atoms in the α -Al₂O₃ substrate escape to the interface and are captured by the C atoms to form the C–O–Al configuration. To further verify the role of high temperature, we subsequently annealed the transferred Gr on α -Al₂O₃ at 1050 °C. We find that such an interfacial C–O–Al configuration can also be observed in this case (Supplementary Fig. 8b), further confirming that the C–O bond is formed at high temperature.

The formation of C–O–Al bonds can significantly change the properties of the interface. The adhesion force/energy of the Gr/ α -Al₂O₃ interface is evaluated using a mechanical nanoscratch method as shown in Supplementary Fig. 10²⁴. The interfacial interaction energy of directly grown Gr on α -Al₂O₃ is ~ 1.47 J m⁻², which is in excellent agreement with our DFT calculations (1.40 J m⁻²). In comparison, the interaction energy of the transferred Gr/ α -Al₂O₃ interface is only ~ 0.66 J m⁻², which is close to the DFT calculation value of 0.46 J m⁻². After high-temperature annealing, the

interaction energy of the transferred Gr increases to ~ 1.25 J m⁻², further confirming the formation of a strong interface bond between Gr and α -Al₂O₃ at high temperature.

Such a strong chemical interaction between Gr and α -Al₂O₃ completely contrasts with the common assumption of vdW interaction^{32,33}. This result provides valuable insight into the remote epitaxy of single-crystalline materials on Gr-coated substrates. The strong interaction between Gr and the substrate (herein, C–O–Al) enables relatively strong atomic interactions from the underlying substrates to penetrate Gr. However, the force between Gr and the epilayer is reduced by nearly two orders of magnitude compared with the covalent bonds formed in the conventional epitaxy approach due to the vdW epitaxy feature¹⁷. In addition, the strong interaction between Gr/ α -Al₂O₃ would create a modulated potential that breaks the symmetry, changes the on-site energy of atoms, and opens up a small band gap around the K-point^{34,35}, which provides promising opportunities for next-generation electronics.

In summary, we obtained the interface structure of Gr/ α -Al₂O₃ by Cs-TEM. We find that the topmost layer is a reconstructed O layer, which directly bonds to Gr to form the C–O–Al interface configuration. In addition, with the presence of Gr and interfacial bonding, the structure relaxation behavior of α -Al₂O₃ near the interface is suppressed compared with that of the bare surface. All these results are in good agreement with the DFT calculations. Our study suggests that the interface of Gr/ α -Al₂O₃ is not as simple as assumed and the interaction between Gr and substrate is a nonpure vdW interaction. The formation of strong bonding between Gr and α -Al₂O₃ is expected to significantly change the optical, electrical, and mechanical properties of Gr. In particular, it provides valuable insights into the remote control of the epitaxy growth of thin films by using Gr as a buffer layer.

Methods

Gr synthesis and transfer. Typically, the commercial α -Al₂O₃ substrate (purchased from Unionlight Technology, Co., Ltd) was loaded into a three-zone high-temperature furnace after the cleaning process. The furnace was heated to 1050 °C and was stabilized for ~ 10 min under 100 s.c.c.m. Ar and 100 s.c.c.m. H₂, and 20 s.c.c.m. CH₄ was introduced into the reaction chamber as a carbon source for the growth of Gr on the α -Al₂O₃ substrate for ~ 3 –5 h.

Transfer of Gr on α -Al₂O₃. The CVD grown Gr on copper is also transferred onto α -Al₂O₃ for comparison, in which process poly (methyl methacrylate) was used as the polymer support³⁶.

Annealing of the transferred sample. The transferred sample was loaded into a high-temperature furnace and heated to 1050 °C, and then annealed for ~ 10 min under the protection of 500 s.c.c.m. Ar, 100 s.c.c.m. H₂.

TEM sample preparation. The Gr/ α -Al₂O₃ TEM specimen was prepared by mechanical polishing followed by argon ion milling (Gatan Model 691 system) with a gun voltage of 1.5–4.5 kV (beam angle of ~ 1.5 –6°). At the final stage of ion milling, the voltage was set at 1.5 kV for ~ 3 min to remove the surface amorphous layer and minimize the damage.

Adhesion force/energy measurement. The adhesion force/energy of the Gr film on α -Al₂O₃ was determined using a mechanical nanoscratch method with the aid of an AFM system (Cypher Asylum Research). The radius of the diamond tip used for the measurement was ~ 40 nm and a normal load of 11.9 μ N was applied.

Data acquisition and analysis. The atomic scale HAADF-STEM images were acquired using a double aberration-corrected FEI (Titan Cubed Themis G2, spatial resolution up to 60 pm) operated at 300 kV with the convergence semiangle 21.5 mrad and collection semiangle snap 80–379 mrad. We also deliberately minimized the electron dose to avoid specimen damage using a small aperture, small beam current, and short scanning time. The atomistic models were generated by VESTA and XCrysDen software. The plots were created by Origin 2018C. Atom positions were determined by simultaneously fitting 2D Gaussian peaks to an a priori perovskite unit cell using a home-developed code running in MATLAB R2012b. The data mapping was also carried out by MATLAB R2012b.

HAADF-STEM image simulation. The multislice STEM simulation was performed using the software pack developed by Kirkland³⁷. We used the single layer Gr/ α -Al₂O₃ interface model shown in Fig. 2. In the simulation, the wave function size, sampling size, and image size were set to 1024 × 1024, 512 × 512, and 512 × 512, respectively. All microscope settings were the same as those in the experiments. The simulated image was then convolved with an 80 pm full width at half maximum Gaussian function considering the incoherent source broadening.

Data availability

All data supporting the findings of this study are available within the paper and its Supplementary Information.

Received: 9 May 2019; Accepted: 9 October 2019;

Published online: 01 November 2019

References

- Kroemer, H. Nobel lecture: quasidelectric fields and band offsets: teaching electrons new tricks. *Rev. Mod. Phys.* **73**, 783–793 (2001).
- Gozar, A. et al. High-temperature interface superconductivity between metallic and insulating copper oxides. *Nature* **455**, 782–785 (2008).
- Reyren, N. et al. Superconducting interfaces between insulating oxides. *Science* **317**, 1196–1199 (2007).
- Ohtomo, A. & Hwang, H. Y. A high-mobility electron gas at the LaAlO₃/SrTiO₃ heterointerface. *Nature* **427**, 423–426 (2004).
- Bibes, M. & Barthélémy, A. Multiferroics: towards a magnetoelectric memory. *Nat. Mater.* **7**, 425–426 (2008).
- Calderon, M. J. et al. Magnetoelectric coupling at the interface of BiFeO₃/La_{0.7}Sr_{0.3}MnO₃ multilayers. *Phys. Rev. B* **84**, 024422 (2011).
- Allain, A., Kang, J., Banerjee, K. & Kis, A. Electrical contacts to two-dimensional semiconductors. *Nat. Mater.* **14**, 1195–1205 (2015).
- Gorbachev, R. et al. Detecting topological currents in graphene superlattices. *Science* **346**, 448–451 (2014).
- Novoselov, K. S., Mishchenko, A., Carvalho, A. & Castro Neto, A. H. 2D materials and van der Waals heterostructures. *Science* **353**, aac9439 (2016).
- Cao, Y. et al. Correlated insulator behaviour at half-filling in magic-angle graphene superlattices. *Nature* **556**, 80–84 (2018).
- Cao, Y. et al. Unconventional superconductivity in magic-angle graphene superlattices. *Nature* **556**, 43–50 (2018).
- Yu, W. J. et al. Highly efficient gate-tunable photocurrent generation in vertical heterostructures of layered materials. *Nat. Nanotechnol.* **8**, 952–958 (2013).
- Venkatesan, B. M. et al. Stacked graphene-Al₂O₃ nanopore sensors for sensitive detection of DNA and DNA–protein complexes. *ACS Nano* **6**, 441–450 (2011).
- Chen, Z. et al. High-brightness blue light-emitting diodes enabled by a directly grown graphene buffer layer. *Adv. Mater.* **30**, 1801608 (2018).
- Qi, Y. et al. Fast growth of strain-free AlN on graphene-buffered sapphire. *J. Am. Chem. Soc.* **140**, 11935–11941 (2018).
- Kim, J. et al. Principle of direct van der Waals epitaxy of single-crystalline films on epitaxial graphene. *Nat. Commun.* **5**, 4836 (2014).
- Kim, Y. et al. Remote epitaxy through graphene enables two-dimensional material-based layer transfer. *Nature* **544**, 340–343 (2017).
- Kong, W. et al. Polarity governs atomic interaction through two-dimensional materials. *Nat. Mater.* **17**, 999–1004 (2018).
- Entani, S. et al. Contracted interlayer distance in graphene/sapphire heterostructure. *Nano Res.* **8**, 1535–1545 (2015).
- Hwang, J. et al. van der Waals epitaxial growth of graphene on sapphire by chemical vapor deposition without a metal catalyst. *ACS Nano* **7**, 385–395 (2012).
- Wang, X. G., Chaka, A. & Scheffler, M. Effect of the environment on α -Al₂O₃ (0001) surface structures. *Phys. Rev. Lett.* **84**, 3650–3653 (2000).
- Yu, R. et al. Direct subangstrom measurement of surfaces of oxide particles. *Phys. Rev. Lett.* **105**, 226101 (2010).
- Gao, P. et al. Atomic-scale measurement of flexoelectric polarization at SrTiO₃ dislocations. *Phys. Rev. Lett.* **120**, 267601 (2018).
- Das, S., Lahiri, D., Agarwal, A. & Choi, W. Interfacial bonding characteristics between graphene and dielectric substrates. *Nanotechnology* **25**, 045707 (2014).
- Silber, D. et al. Adsorbate-induced lifting of substrate relaxation is a general mechanism governing titania surface chemistry. *Nat. Commun.* **7**, 12888 (2016).
- Price, D. L., Wills, J. M. & Cooper, B. R. TIC (001) surface relaxation. *Phys. Rev. Lett.* **77**, 3375–3378 (1996).
- Ishikawa, K. & Uemori, T. Surface relaxation in ferroelectric perovskites. *Phys. Rev. B* **60**, 11841–11845 (1999).
- Kim, J. H. et al. Growth of heteroepitaxial ZnO thin films on GaN-buffered Al₂O₃ (0001) substrates by low-temperature hydrothermal synthesis at 90 °C. *Adv. Funct. Mater.* **17**, 463–471 (2007).
- Tuan, A. C. et al. Epitaxial growth and properties of cobalt-doped ZnO on α -Al₂O₃ single-crystal substrates. *Phys. Rev. B* **70**, 054424 (2004).
- Prellier, W., Fouchet, A., Mercey, B., Simon, C. & Raveau, B. Laser ablation of Co: ZnO films deposited from Zn and Co metal targets on (0001) Al₂O₃ substrates. *Appl. Phys. Lett.* **82**, 3490–3492 (2003).
- Toofan, J. & Watson, P. The termination of the α -Al₂O₃ (0001) surface: a LEED crystallography determination. *Surf. Sci.* **401**, 162–172 (1998).
- Liu, Y. et al. Van der Waals heterostructures and devices. *Nat. Rev. Mater.* **1**, 16042 (2016).
- Wang, Y. et al. Van der Waals contacts between three-dimensional metals and two-dimensional semiconductors. *Nature* **568**, 70–74 (2019).
- Zhou, S. Y. et al. Substrate-induced bandgap opening in epitaxial graphene. *Nat. Mater.* **6**, 770–775 (2007).
- Pisana, S. et al. Breakdown of the adiabatic Born–Oppenheimer approximation in graphene. *Nat. Mater.* **6**, 198–201 (2007).
- Suk, J. W. et al. Transfer of CVD-grown monolayer graphene onto arbitrary substrates. *ACS Nano* **5**, 6916–6924 (2011).
- Kirkland, E. J. *Advanced Computing in Electron Microscopy* (Springer Science & Business Media, 2010).

Acknowledgements

The work was supported by the National Key R&D Program of China (Grant Numbers 2018YFB0406703 and 2018YFB2202801), the National Natural Science Foundation of China (Grant Numbers 51672007, 11974023, 61851403, and 61427901), The Key R&D Program of Guangdong Province (2018B030327001 and 2018B010109009), the National Equipment Program of China (ZDYZ2015-1), and the “2011 Program” Peking-Tsinghua-IOP Collaborative Innovation Center for Quantum Matter. We acknowledge Electron Microscopy Laboratory in Peking University for the use of Cs-corrected electron microscope. The DFT calculations were carried out on TianHe-1(A) at the National Supercomputer Center in Tianjin.

Author contributions

P.G., S.Y. and L.L. conceived the idea and designed the experiments. Z.D. and Y.S. prepared the TEM cross-sectional sample and did the STEM characterization assisted by Y.L., B.L. and Q.L. N.L. did the quantitative image analysis. S.Y. did the density functional theory calculations. Z.C. are responsible for technical assistance with graphene growth, Raman characterization, and XPS measurements under direction of Z.F.L. Z.Y. and T.M. performed the adhesion force/energy measurement. Z.D. and Z.C. performed the data analysis and wrote the manuscript under the direction of P.G. All authors contributed to the discussion and analysis of the results.

Competing interests

The authors declare no competing interests.

Additional information

Supplementary information is available for this paper at <https://doi.org/10.1038/s41467-019-13023-6>.

Correspondence and requests for materials should be addressed to S.Y., L.L. or P.G.

Peer review information *Nature Communications* thanks Qinghong Yuan and the other, anonymous, reviewer(s) for their contribution to the peer review of this work.

Reprints and permission information is available at <http://www.nature.com/reprints>

Publisher's note Springer Nature remains neutral with regard to jurisdictional claims in published maps and institutional affiliations.



Open Access This article is licensed under a Creative Commons Attribution 4.0 International License, which permits use, sharing, adaptation, distribution and reproduction in any medium or format, as long as you give appropriate credit to the original author(s) and the source, provide a link to the Creative Commons license, and indicate if changes were made. The images or other third party material in this article are included in the article's Creative Commons license, unless indicated otherwise in a credit line to the material. If material is not included in the article's Creative Commons license and your intended use is not permitted by statutory regulation or exceeds the permitted use, you will need to obtain permission directly from the copyright holder. To view a copy of this license, visit <http://creativecommons.org/licenses/by/4.0/>.

© The Author(s) 2019